

## Research Article

# Study of Magnetic, Optical, Electronic and Thermodynamic Effects in Thallium Rare Earth Disulphides (TIRES<sub>2</sub>, RE= Tb- Er)

Annveer<sup>2</sup>, Rahul Gautam<sup>1</sup>, Rishi P. Singh<sup>1\*</sup>, Arvind Kumar<sup>3</sup>, Praveen Kumar<sup>1</sup>

<sup>1</sup>Quantum computational Lab, Department of Physics, S.S.V. College (Hapur) affiliated to CCS University, Meerut-India

<sup>2</sup>Department of Physics, N.R.E.C. College (Khurja), CCS University, Meerut-India

<sup>3</sup>Department of Physics, A.R.S.D. College, University of Delhi-India

E-mail: rishisingh79@gmail.com; drpsinghphy@ssvpgcollege.org

**Received:** 16 April 2023; **Revised:** 29 May 2023; **Accepted:** 5 June 2023

**Abstract:** In the present research work, we have investigated density of electronic states, electronic band structure, magnetic structure, optical spectra and temperature dependent thermodynamic characteristics of thallium rare earth sulphides, TIRES<sub>2</sub> (RE: Tb-Er) using FP-LAPW method and PBE-GGA exchange correlation within DFT. The electronic structure pointed out that TIRES<sub>2</sub> compounds show half metallic character. The magnetic moment and spin polarization calculations prove that TIRES<sub>2</sub> are fully spin polarized compounds with ferromagnetic nature. Optical spectra show that intraband transitions occur in infrared (IR) regime due to half metallic character of TIRES<sub>2</sub> and behave as opaque in ultraviolet (UV) region. High refractive index in IR regime also show metallic character and high peak in UV regime show slow propagation of light in UV regime. The reflection coefficient is found maximum (~50–60%) in UV regime. Greater energy loss has been seen on the higher energy side, which corresponds to the stimulation of plasmons by electrons moving through the compounds. Plasma resonances lead to the frequent peaks at ~ 6.0 eV, 11.0 eV, and 12.0 eV. According to calculations made using the quasi-harmonic Debye model, TIRES<sub>2</sub> compounds are dimensionally less stable (i.e., much hard), have poor thermal conductivity, and experience faster-than-average disorder with increasing the temperature.

**Keywords:** half metallics; electronic structure; optical properties; thermodynamic properties

## 1. Introduction

Half metals are the substances that act as a conductor to one type electron spin orientation (either spin up or spin down) and acts as semiconductor or insulator to the opposite type of spin orientation and considered as hybrid of metals and semiconductors [1, 2]. Most of the half metallic materials are fully spin polarized and show the ferromagnetic character [3]. These characteristics motivate us to look for new, appropriate spin-dependent materials that may be used to make electronic and magnetic devices, such as spin valves, giant magneto-resistance, tunnelling magneto-resistance, and non-volatile magnetic random access memory [4, 5].

The study of optical properties of metals/half metals shows that absorption of free carrier is important in half metals for which intraband transitions occur in infrared regime [6]. However, in semimetals the carrier densities are almost independent of temperature but high mobility of carriers provides the large optical conductivity [7]. Half metals basically show metallic characteristics towards the thermodynamic properties but they are generally less conductors of heat and electricity compared to the metals and they are usually malleable and ductile [8].

The research here looked at thallium rare earth sulphides, TIRES<sub>2</sub> (RE = rare earth elements: Tb, Dy, Ho, Er,) have been chosen for the electronic, magnetic, optical and thermodynamic properties. The basic structural

Copyright ©2023 Annveer, et al.

DOI: <https://doi.org/10.37256/mp02010004>

This is an open-access article distributed under a CC BY license  
(Creative Commons Attribution 4.0 International License)

<https://creativecommons.org/licenses/by/4.0/>

parameters of Tl(Tb/Dy/Ho/Er)S<sub>2</sub> have been displayed in Table 1. Table 1 indicates that thallium rare earth disulphides materials adopt  $\alpha$ -NaFeO<sub>2</sub> type rhombohedral structure with space group  $R\bar{3}m$  and consist of magnetic ions layers separated by three layers of non-magnetic ions [9, 10]. In the present study, electronic and magnetic structure reveal that Tl(Tb/Dy/Ho/Er)S<sub>2</sub> are half metallic materials with 100% spin polarization at Fermi level. All TlRES<sub>2</sub> compounds show ferromagnetic character. Thus, studied compounds, Tl(Tb/Dy/Ho/Er)S<sub>2</sub> may be considered as half metallic ferromagnets. These compounds may be good alternatives of conventional half metallic materials that may be used in making new magnetic/electronic device applications. They may show also important characteristics towards the optical properties for new optical device applications. Thus, Tl(Tb/Dy/Ho/Er)S<sub>2</sub> compounds have been chosen for electronic, magnetic, optical and thermodynamic studies for better understanding towards further applications.

**Table 1.** Unit Cell Parameters (Å), Space Group, structure type and atomic coordinates of TlRES<sub>2</sub>, RE=Tb-Er

Compounds	Unit Cell Parameters (Å) (Expt.) [21]		Unit Cell Parameters (Å) (Calculated)		Space Group and Structure Type	Atomic Coordinates
	a <sub>0</sub>	c <sub>0</sub>	a <sub>0</sub>	c <sub>0</sub>		
	TlTbS <sub>2</sub>	4.020	2.224	4.000		
TlDyS <sub>2</sub>	3.998	2.241	3.974	2.233	$\alpha$ -NaFeO <sub>2</sub> type	RE:(0.5, 0.5, 0.5)
TlHoS <sub>2</sub>	4.011	2.249	4.001	2.232	$\alpha = \beta = 90$	RE = Nd, Tb, Dy, Ho, Er, Tm, Yb
TlErS <sub>2</sub>	3.961	2.244	3.932	2.2301	$\gamma = 120$	Te:(0.23344, 0.23344, 0.23344)

In accordance with the literature, three compounds with the same crystal structure such as thallium gadolinium chalcogenides TlGd(S<sub>2</sub>/Se<sub>2</sub>/Te<sub>2</sub>), have been examined by Gautam et al [11] for their electronic, magnetic, thermodynamic, and transport characteristics. They found that TlGdS<sub>2</sub> is an indirect wide band gap semiconductor with bandgap 1.86 eV and it has Seebeck coefficient  $\sim 89 \mu\text{V/K}$  and electrical conductivity  $\sim 267 \Omega\text{cm}^{-1}$  [11]. Sankar et al studied the thermoelectric properties of TlGd(S<sub>2</sub>/Se<sub>2</sub>/Te<sub>2</sub>) [9]. Duczmal et al. investigated the structural and magnetic characteristics of TlGd(S<sub>2</sub>/Se<sub>2</sub>/Te<sub>2</sub>) [12, 13]. Guseinov et al. [14] investigated the physical properties of various rare earth and thallium based chalcogenides.

In our present study, our objective and effort is in the same direction to explore the systematic characteristics of electronic band structure, electronic density of states, magnetic, thermodynamic and optical properties of TlRES<sub>2</sub> for further understanding and controlling the properties for different applications.

## 2. Computational method and structural details

The FP-LAPW / PP-PW technique [15] under density functional theory (DFT) [16] as implemented in the WIEN2k and VASP code, respectively [17, 18] have been used in this study to examine the electronic, magnetic, thermodynamic, and optical characteristics of thallium rare earth disulphides. The calculations have been done using the exchange-correlation potential, PBE-GGA based on Perdew et al. [19]. Within the non-overlapping muffin-tin spheres enclosing the atomic sites, Kohn-Sham wave functions [20] were enlarged in terms of spherical harmonic functions. We have used the plane wave cut off ( $R_{MT}K_{max}$ ) = 6 under convergence limit for the calculation where  $K_{max}$  is the plane wave cut-off energy and  $R_{MT}$  is known for the smallest radii of all atomic spheres. The calculations have been made with an energy accuracy limit of 0.0001 Ry and the cut-off energy  $-6.0$  Ry. The density of the 1,000  $k$ -points has been selected in the Brillouin Zone to determine the electronic, magnetic, thermodynamic, and optical characteristics of TlRES<sub>2</sub> compounds.

The optical properties of the compounds promote for the development of new optoelectronic devices. The complex dielectric function  $\varepsilon(\omega)$  is a unique approach for the investigation of optical properties. It explores the linear response of compounds with an external electromagnetic field [20–24]. The complex dielectric function is sum of real and imaginary part of dielectric function (i.e., sum of  $\varepsilon_1(\omega)$  and  $\varepsilon_2(\omega)$ ) which gives the information about the dispersion and absorption behaviour of material respective complex dielectric function is expressed as [21–25].

$$\varepsilon(\omega) = \varepsilon_1(\omega) + i\varepsilon_2(\omega)$$

Random phase approximation provides the imaginary part of the dielectric function which is expressed as;

$$\varepsilon_2(\omega) = \frac{4\pi e^2}{m^2 \omega^2} \sum_{i,j} |M_{ij}|^2 f_i(1-f_j) \times \delta(E_F - E_i - \omega) d^3k \quad (1)$$

Here  $M$  represents the dipole matrix element and  $f_i$  indicates the Fermi distribution function in  $i^{\text{th}}$  state.  $E_i$  show the energy of electron in the  $i^{\text{th}}$  states.

Kramers-Kronig relation gives the real part,  $\varepsilon_1(\omega)$  of dielectric function, represented as [21–25]:

$$\varepsilon_1(\omega) = 1 + \frac{2}{\pi} P \int_0^\infty \frac{\omega' \varepsilon_2(\omega')}{(\omega^2 - \omega'^2)} d\omega' \quad (2)$$

Here,  $P$  implies the principal value of the integral.

The following equations may also be used to get residual key optical properties like as the absorption coefficient,  $\alpha(\omega)$ , refractive index,  $n(\omega)$ , reflectivity,  $R(\omega)$ , extinct coefficient,  $k(\omega)$ , and energy loss,  $L(\omega)$ ; [21–25]:

$$\alpha(\omega) = \sqrt{2\omega} \left[ \sqrt{\varepsilon_1^2(\omega) + \varepsilon_2^2(\omega)} - \varepsilon_1(\omega) \right]^{1/2} \quad (3)$$

$$R(\omega) = \frac{(\eta - 1)^2 + k^2}{(\eta + 1)^2 + k^2}, \quad (4)$$

Where,  $n$  and  $k$  stand for the real and fictitious portions of the complicated refractive index.

$$\eta(\omega) = \frac{\sqrt{\varepsilon_1^2(\omega) + \varepsilon_2^2(\omega)} + \varepsilon_1(\omega)}{\sqrt{2}} \quad (5)$$

$$k(\omega) = \frac{\sqrt{\varepsilon_1^2(\omega) + \varepsilon_2^2(\omega)} - \varepsilon_1(\omega)}{\sqrt{2}} \quad (6)$$

$$L(\omega) = \frac{\varepsilon_2(\omega)}{[\varepsilon_1^2(\omega) + \varepsilon_2^2(\omega)]} \quad (7)$$

### 3. Results and discussion

#### 3.1 Electronic and magnetic effects

Densities of states (DOS) and band structure play an important role in determining the physical behaviour such as metallic/semiconducting/insulating behaviour of crystalline compounds. The total DOS of TIRES<sub>2</sub> (RE: Tb - Er) have been explored in the Figures 1(a–d) in which dotted line at 0 eV shows the Fermi level. It is clear from Figures 1(a–d) that spin up channel of TIRES<sub>2</sub> compounds show a wide gap between valance states and conduction states (i.e. spin up states show insulating character) whereas significant density of states of spin down channel are crossing the Fermi level (i.e. spin down states show metallic character). Thus, Tl(Tb/Dy/Ho/Er)S<sub>2</sub> compounds show half metallic nature.

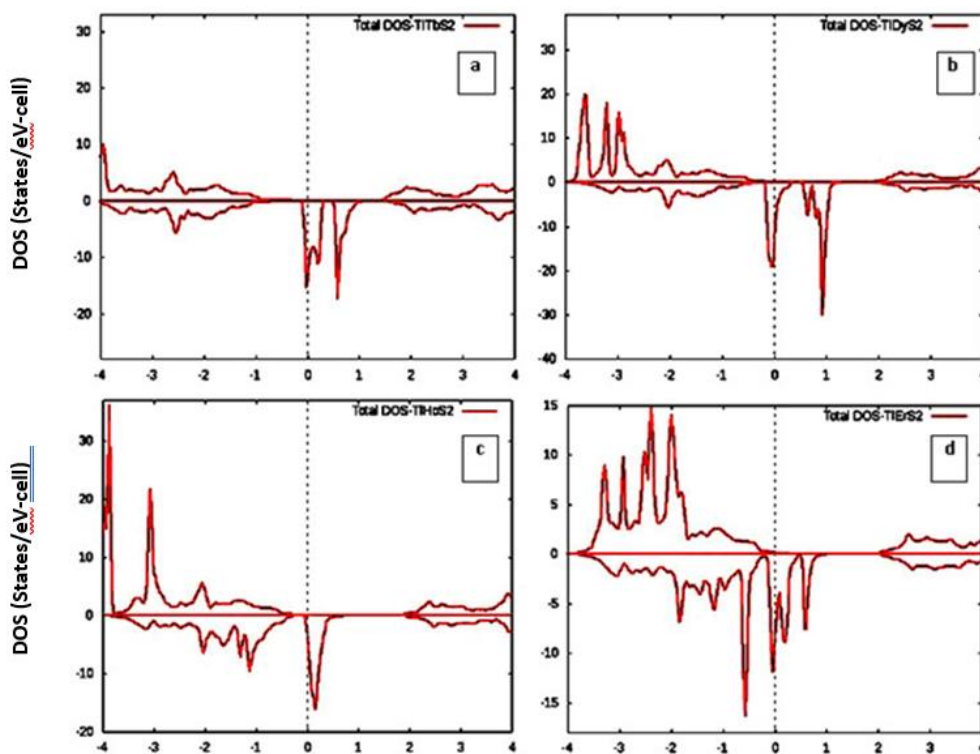


**Figure 1.** Total density of states for (a) TITbS<sub>2</sub> (b) TIDyS<sub>2</sub> (c) TIHoS<sub>2</sub> (d) TIERS<sub>2</sub>

To describe which atom mainly take a part in half metallic character of the compounds, total and partial density of states for separate constituent atoms of TITbS<sub>2</sub> have been shown Figures 2(a–h) (The DOS plots for Tl/(Dy/Ho/Er)S<sub>2</sub> have not been demonstrated in this manuscript because they consists of similar features as that of TITbS<sub>2</sub>). It can be seen from Figures 2(b) and 2(g) that at the Fermi level, *Tb-f* states have contributed mainly to give metallic character to TITbS<sub>2</sub> (with dominance of spin down channel of *Tb-f* states or RE= (Dy/Ho/Er)-*f* states atoms in the compounds Tl(Tb/Dy/Ho/Er)S<sub>2</sub>). These states are also responsible for magnetic moment in TITbS<sub>2</sub> (or TIERS<sub>2</sub>) as *Tb-f* (or RE-*f*) states are existed at different positions of energy for opposite spins (at ~ -5.0 eV for spin up and between 0 to 1 eV energy region for spin down states). Thus, in Tl(Tb/Dy/Ho/Er)S<sub>2</sub> compounds *f*-orbital electrons of RE= Tb/Dy/Ho/Er atoms provide the half metallic character as well as magnetic character to TIERS<sub>2</sub> compounds.

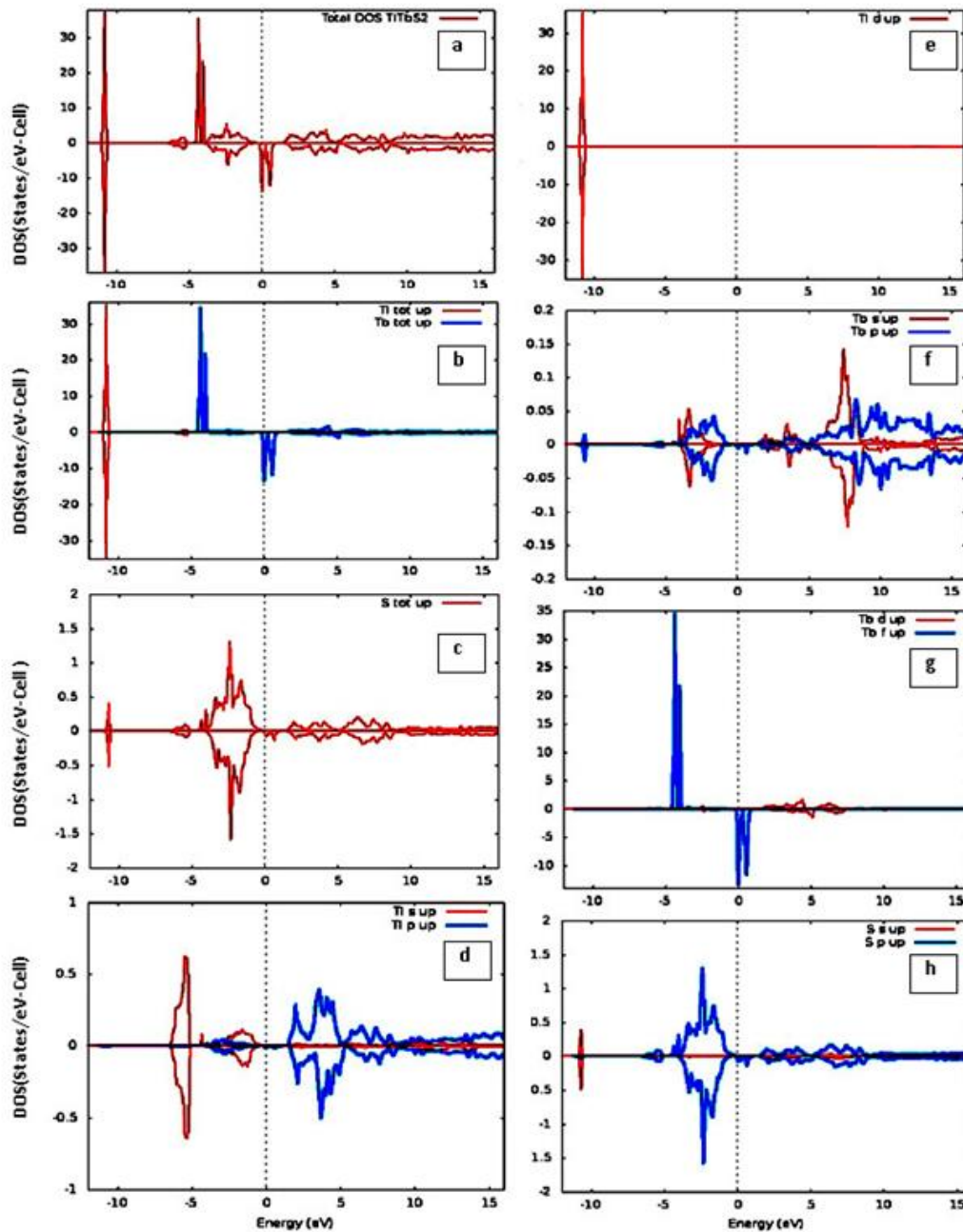


**Figure 2.** Total and partial density of states for (a) TlTbS<sub>2</sub> (b) Tl-Total and Tb-Total (c) S-Total (d) Tl-s and Tl-p orbital (e) Tl-d orbital (f) Tb-s and Tb-p orbital (g) Tb-d orbital and Tb-f orbital (h) S-s and S-p orbital

In order to verify the half metallic nature and magnetic character of TlTbS<sub>2</sub>; band structure diagram for spin up and spin down bands for TlTbS<sub>2</sub> have been shown in Figures 3(a, b). The band structure diagrams of Tl/(Dy/Ho/Er)S<sub>2</sub> have not been displayed because they contain similar character as that of TlTbS<sub>2</sub>. It is clear from Figures 3(a, b) that TlTbS<sub>2</sub> show a band gap between Fermi level and spin up conduction bands while there is zero gap for spin dn bands at the Fermi level, verify half metallic character and justify also our DOS calculations.

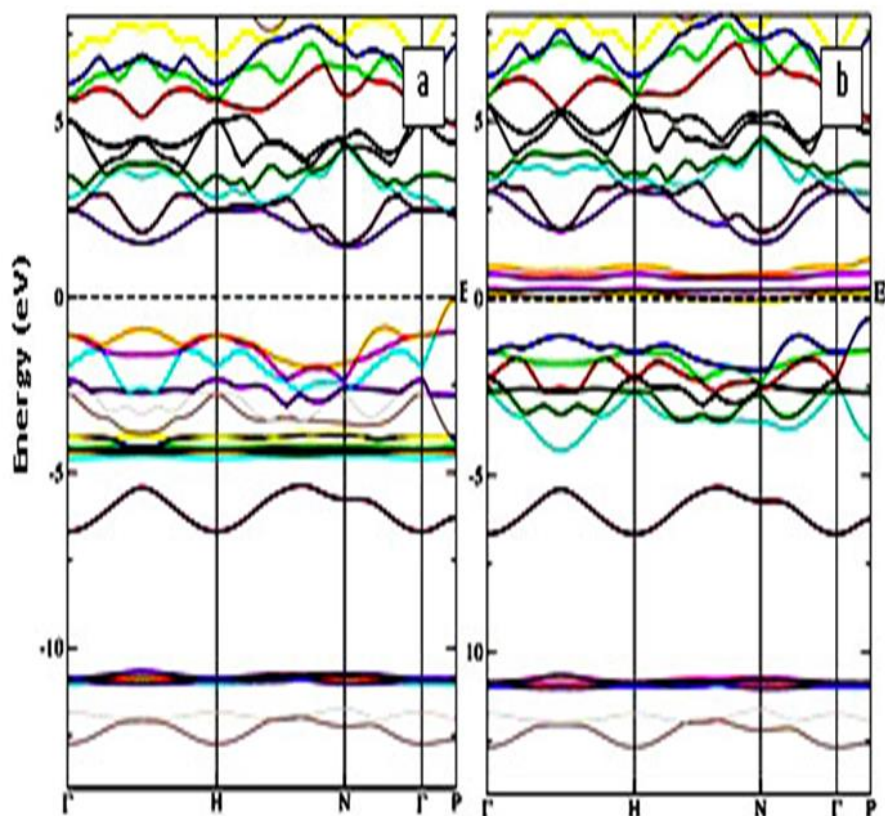


**Figure 3.** Electronic band structure along the high symmetry directions  $\Gamma$ , H, N and P for (a) TITbS<sub>2</sub>-up (b) TITbS<sub>2</sub>-dn

The magnetic character viz. magnetic moment, electron spin polarization of the compounds can be extracted from the spin polarized DOS calculations. The calculated total and partial magnetic moment on constituent atoms of TIREs<sub>2</sub> and electron spin polarization have been displayed in Table 2. It can be observed from Table 2 that magnetic moment of interstitial region, TI and S atoms is negligible compared to the magnetic moment of corresponding RE atoms, indicate dominant contribution of corresponding RE atoms in total magnetic moment of TIREs<sub>2</sub> compounds.

The calculated total magnetic moment has been compared with available experimental values [26] only for TIErS<sub>2</sub> compound because no experimental values [25] of total magnetic moment for other compounds viz. TI(Tb/Dy/Ho)S<sub>2</sub> has been reported in the literature. It is clear from Table 2 that calculated values of magnetic moment for TIErS<sub>2</sub> compound is nearly close to available experimental values, justify our magnetic calculations.

**Table 2.** Magnetic moment,  $\mu_B$  Magnetization, M ( $\mu_B$ ) Fermi energy  $E_0$  (eV) at equilibrium condition (at 0 K) for TIREs<sub>2</sub>, RE=Tb-Er using PBE-GGA

Compounds	$\mu_B^{\text{Interstitial}}$	$\mu_B^{\text{TI}}$	$\mu_B^{\text{TNd/Gd/Tb/Dy/Ho/Er/Tm/Yb}}$	$\mu_B^{\text{S}}$	$\mu_B^{\text{total}}$
TITbS <sub>2</sub>	0.0712	0.0024	7.8789	0.0252	7.9777
TIDyS <sub>2</sub>	0.0570	0.0021	7.8904	0.0421	7.9916
TIHoS <sub>2</sub>	0.0582	0.0049	8.9044	0.0440	9.0115
TIErS <sub>2</sub>	0.0589	0.0056	7.8645	0.0610	7.9900 (9.52)*

\*Duczmal, Marek, Structure, magnetic properties and crystal field in triple lanthanide chalcogenide and thallium TILnX<sub>2</sub> (X = S, Se or Te), Publishing House of the Wrocław University of Technology, Wrocław 2003

Now, electrons spin polarization,  $\delta$  can be calculated by the formula [27]:

$$\delta = \frac{\delta \uparrow - \delta \downarrow}{\delta \uparrow + \delta \downarrow} \quad (8)$$

Where,  $\delta \uparrow$  and  $\delta \downarrow$  displays the density of states for spin up electrons as well as the spin up electrons at the Fermi level.

The calculated value of  $\delta$  using equation (8) is found to be 1 for all Tl(Tb/Dy/Ho/Er)S<sub>2</sub> compounds as  $\delta \uparrow = 0$  for Tl(Tb/Dy/Ho/Er)S<sub>2</sub> compounds at the Fermi level. Again, it is noticeable here that unit value of  $\delta$  leads to 100% spin polarization [27] at the Fermi level i. e., TIRES<sub>2</sub> compounds are fully spin polarized which is basic condition of half metallic compounds [27].

### 3.2 Optical effects

Dielectric function,  $\epsilon(\omega)$  is an important parameter which describes the optical behavior of a material under an external electromagnetic field. It consists of two parts: real part,  $\epsilon_1(\omega)$  and imaginary part,  $\epsilon_2(\omega)$ . Real part,  $\epsilon_1(\omega)$  describes the dispersion of electromagnetic radiation when it is propagated in the material i.e., polarization of light. Imaginary part,  $\epsilon_2(\omega)$  represents the absorption of energy of incident photons into the material i.e., loss of energy [23, 24, 28]. Figures 4(a–d) show the variation of real part of the dielectric function ( $h\nu$ ) along two different crystallographic x- and z-directions, calculated for the TIRES<sub>2</sub> (RE=Tb-Er) compounds, respectively. It is well known that intraband transitions are effective in IR region for metallic materials [23, 24, 28]. It is clear from Figures 4(a–d) that presence of  $\epsilon_1(\omega)$  values close to 0 eV in IR region (0.01 eV–1.7 eV) are owing to intraband transitions that confirm the half metallic character of TIRES<sub>2</sub> due to spin down states near the Fermi level. Now,  $\epsilon_1(\omega)$  starts to increase from visible region (1.7 eV–3.3 eV) and maximize at ~ 4.0 eV, in near ultraviolet (UV) region indicate that TIRES<sub>2</sub> compounds have highest optical response in UV region. Furthermore, after 4.0 eV,  $\epsilon_1(\omega)$  decreases and become negative at around 5.0 eV for all the compounds. The negative value of  $\epsilon_1(\omega)$  after ~ 5.0 eV represents the opaque region for the electromagnetic radiation. The variation of  $\epsilon_1(\omega)$  also demonstrate that anisotropy is maximum at either 0 eV or at ~ 4.0 eV in  $\epsilon_1(\omega) \geq 0$  region and at ~ 6.0 eV in  $\epsilon_1(\omega) < 0$  for all TIRES<sub>2</sub> compounds.

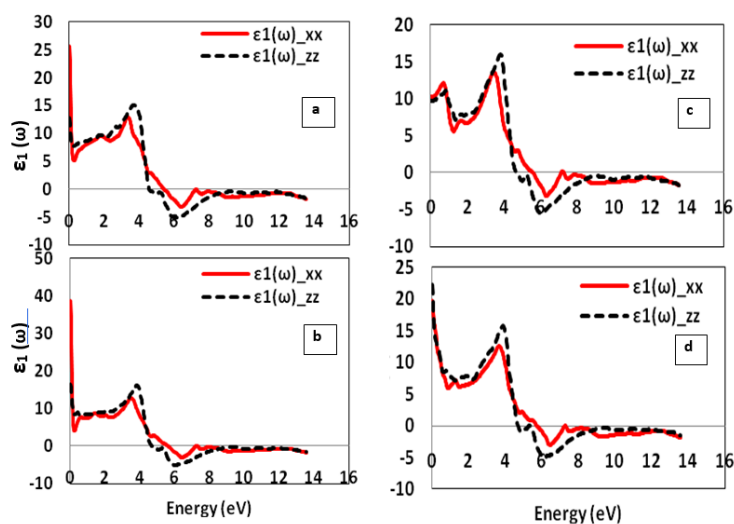


**Figure 4.** Variation of Real part of dielectric function,  $\epsilon_1(\omega)$  along x- and z- directions for (a) TlTbS<sub>2</sub> (b) TlDyS<sub>2</sub> (c) TlHoS<sub>2</sub> (c) TlErS<sub>2</sub>

Imaginary part of the dielectric constant,  $\epsilon_2(\omega)$  represents the loss part of incident photons energy or energy absorbed by the material [28]. The variation of  $\epsilon_2(\omega)$  with photon energy have been shown Figures 5 (a–d) for TIRES<sub>2</sub> compounds along x- and z-directions. It is clear from Figures 5(a–d) that first probable loss occurs close to 0 eV in IR region for Tl(Tb/Dy/Ho/Er)S<sub>2</sub> compounds, implies metallic character (which indicates transition of intraband by using the incident low photon energy) which are well correlated to density of states and band structure calculations. The most probable highest peaks in energy range 3.0 eV–6.0 eV along x- and z-axis and at ~ 5.0 eV along z-axis show interband transition of electrons among occupied to unoccupied energy levels. Furthermore, however some peaks with low intensity were observed below 3.0 eV and above 6.0 eV but the maxima peaks

(highest peaks) have been found in near ultraviolet region (above 3.3–7.0 eV). Thus, these materials can be supposed to make more useful in optoelectronic devices for near ultraviolet light.

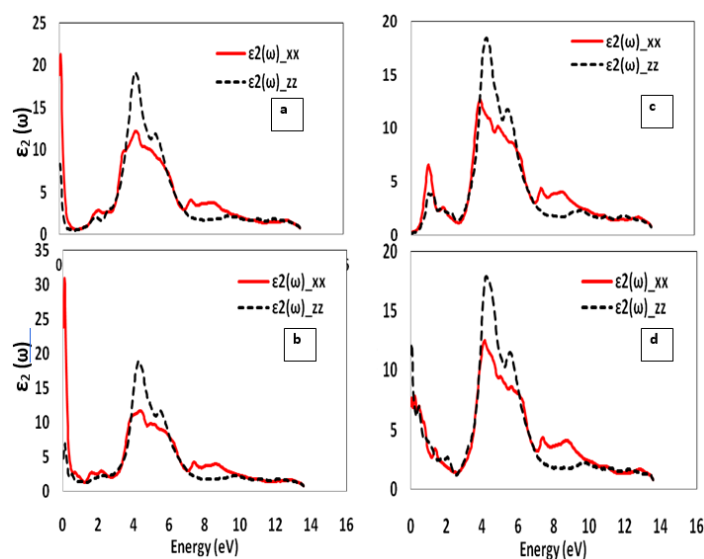


**Figure 5.** Variation of imaginary part,  $\epsilon_2(\omega)$  of dielectric function along x- and z- directions for (a) TlTbS<sub>2</sub> (b) TlDyS<sub>2</sub> (c) TlHoS<sub>2</sub> (d) TlErS<sub>2</sub>

Figures 6(a–d) display the variation of refractive index,  $n(\omega)$  with photon energy for TlErS<sub>2</sub> materials. It is clear from the Figures 6 (a–d) that refractive index,  $n(\omega)$  has large value at 0 eV and in region less than 1.0 eV. This is due to existence *RE-4f* electrons of spin down states that are attributed to metallic character of Tl(Tb/Dy/Ho/Er)S<sub>2</sub>. Beyond 1 eV,  $n(\omega)$  increases in the visible range and a highest peak appears in the near UV region at around 4.0 eV along both the x- and z-axis, confirm slow propagation of velocity of light in UV region. The Penn Model links the real component of the dielectric constant  $\epsilon_1(\omega)$  to the refractive index,  $n(\omega)$  by the relation  $n^2(\omega) = \epsilon_1(\omega)$  [29]. It can be seen from Table 3 that our estimated values of refractive index,  $n(\omega)$  satisfy the Penn model, authenticate the accuracy of our calculations for the compounds.

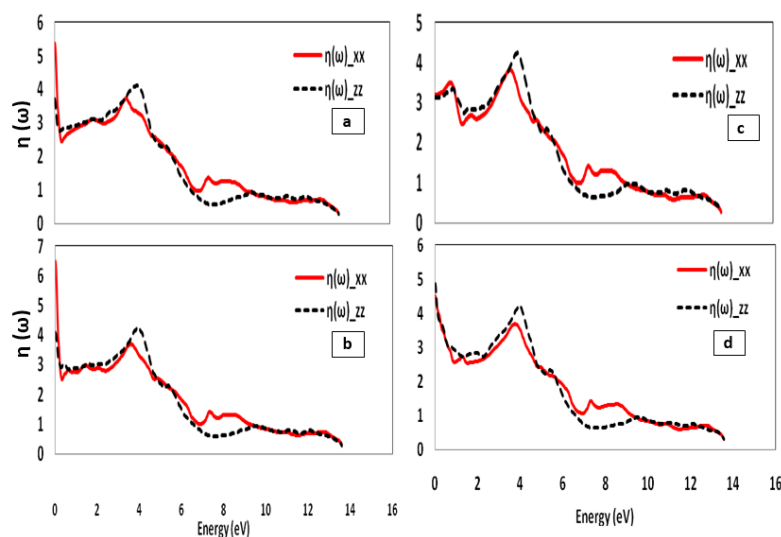


**Figure 6.** Variation of refractive index,  $\eta(\omega)$  with photon energy along x- and z- directions for (a) TlTbS<sub>2</sub> (b) TlDyS<sub>2</sub> (c) TlHoS<sub>2</sub> (d) TlErS<sub>2</sub>

**Table 3.** Refractive index,  $\eta(\omega)$  calculated using spectra and Pen model along x- and z- direction for TlErS<sub>2</sub>, RE=Tb–Er using PBE-GGA

Compounds	By using Spectra	By using Pen model
-----------	------------------	--------------------

	$\eta^{xx}(\omega)$	$\eta^{zz}(\omega)$	$\eta^{xx}(\omega)$	$\eta^{zz}(\omega)$
<b>TlTbS<sub>2</sub></b>	5.4	3.9	5.02	3.67
<b>TlDyS<sub>2</sub></b>	6.5	4.20	6.24	4.12
<b>TlHoS<sub>2</sub></b>	3.3	3.20	3.31	3.16
<b>TlErS<sub>2</sub></b>	4.8	4.6	4.47	4.79

Figures 7(a–d) show variation extinction coefficient,  $k(\omega)$  which is an imaginary part of refraction function. Extinction co-efficient,  $k(\omega)$  is related to refractive index and dielectric constants as;  $n^2 - k^2 = \epsilon_1(\omega)$  and  $2nk = \epsilon_2(\omega)$  [30]. For metallic materials,  $n(\omega)$  is much lower than extinction coefficient in the low energy range due to free electron carriers' effect [29]. The high peak of  $k(\omega)$  at  $\sim 4.0$  eV and 6.0 eV shows maximum absorption of photons in UV region as  $k(\omega)$  also show the absorption of incident radiation.

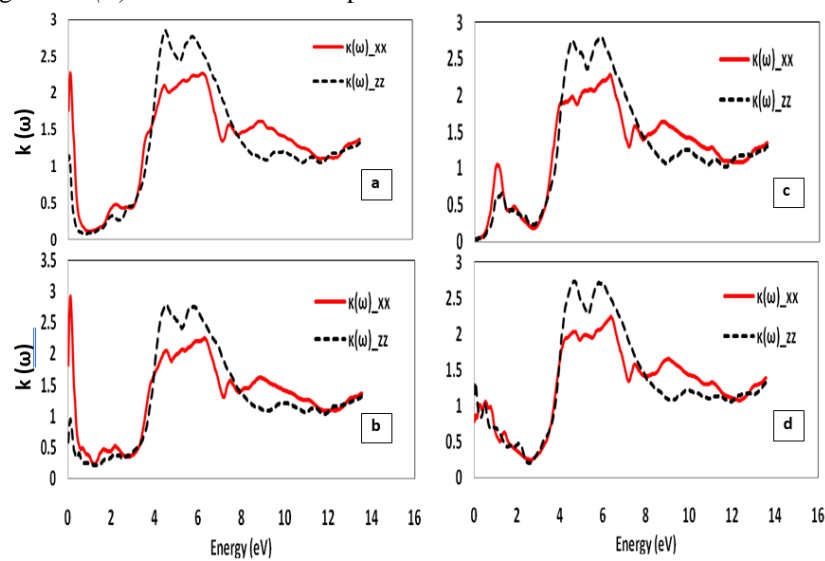


**Figure 7.** Variation of extinction coefficient,  $k(\omega)$  with photon energy along x- and z- directions for (a) TlTbS<sub>2</sub> (b) TlDyS<sub>2</sub> (c) TlHoS<sub>2</sub> (d) TlErS<sub>2</sub>

Figures 8(a–d) show how the reflection spectra change along the two distinct crystallographic axes as a function of photon energy. The high values of static reflection coefficient  $\sim 50\%$  to  $60\%$  for Tl(Tb/Dy/Ho/Er)S<sub>2</sub> give attention that these compounds are half metallic. Furthermore, reflectivity is larger along z-direction compared to x-direction in energy range  $\sim 3$ - $8$  eV and reverse effect is obtained beyond  $8.0$  eV. The highest peaks of reflection coefficient ( $50\%$ – $60\%$ ) in  $\sim 3$ - $8$  eV energy regime show large reflectance in UV region.

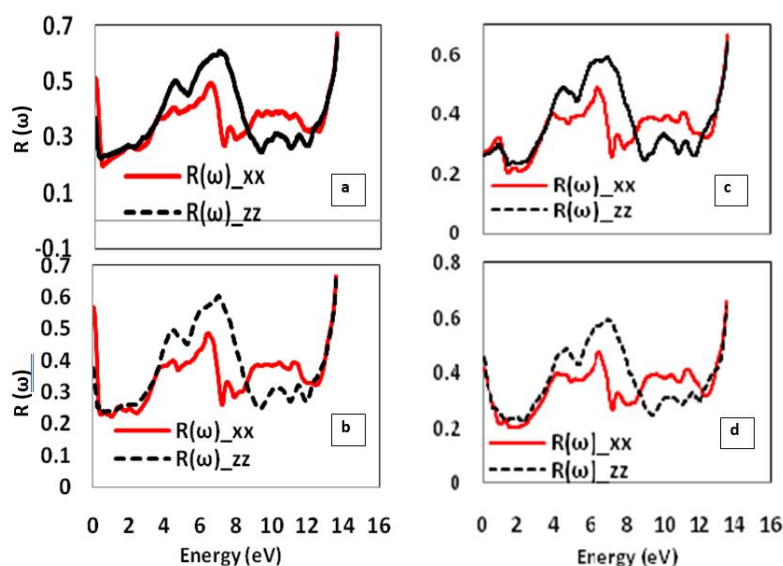


**Figure 8.** Variation of reflection spectra,  $R(\omega)$  with photon energy along x- and z- directions (a) TITbS<sub>2</sub> (b) TIDyS<sub>2</sub> (c) TIHoS<sub>2</sub> (d) TIErS<sub>2</sub>

Absorption coefficient measures the rate of decrease in intensity of light when it propagates in to the material. Figures 9(a–d) show the variation of absorption coefficient,  $\alpha(\omega)$  with photon energy. It can be observed from Figures 9(a–d) that absorption edge for Ti(Tb/Dy/Ho/Er)S<sub>2</sub> begins from low photon energy in IR regime (indicate metallic nature of TIRES<sub>2</sub>). After IR regime,  $\alpha(\omega)$  rises up in the visible region and maximize in ultraviolet regime (UV) at ~6.0 eV. In the IR domain, the low value of  $\alpha(\omega)$  reveals that TIRES<sub>2</sub> are less absorbent and behave as transparent materials, but the high value of  $\alpha(\omega)$  at 6.0 eV in the UV regime demonstrates that these materials are more absorbent and behave as opaque materials.

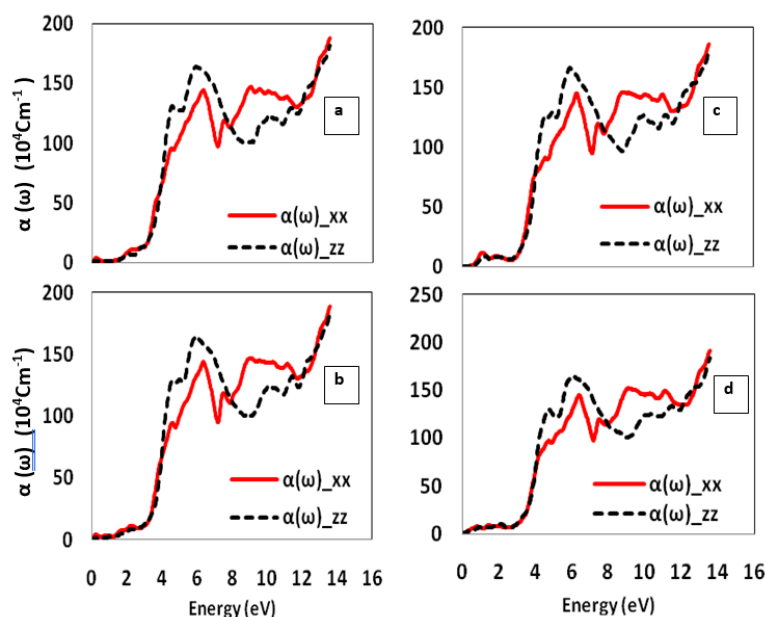


**Figure 9.** Variation of absorption coefficient,  $\alpha(\omega)$  with photon energy along x- and z- directions (a) TITbS<sub>2</sub> (b) TIDyS<sub>2</sub> (c) TIHoS<sub>2</sub> (d) TIErS<sub>2</sub>

The variation of optical conductivity,  $\sigma(\omega)$  with photon energy for the studied compounds have been shown in Figures 10 (a–d), along two different crystallographic x- and z- directions. These graphs demonstrate that variations in conductivity exhibit the same pattern as the imaginary portion of dielectric constants because  $\sigma(\omega)$  and  $\epsilon_2(\omega)$  are connected by the following equation:  $\sigma(\omega) = (\omega/4\pi)\epsilon_2$  [31, 32]. Sharp peaks in the energy ranges of ~3–6 eV and ~7–10 eV have been seen in both directions, and these peaks are due to these materials transition from occupied to unoccupied states. The abrupt high peak at 5.0 eV shows that the examined compounds are more photon absorbent in the UV region and exhibit their greatest photon absorbent behaviour at this energy.

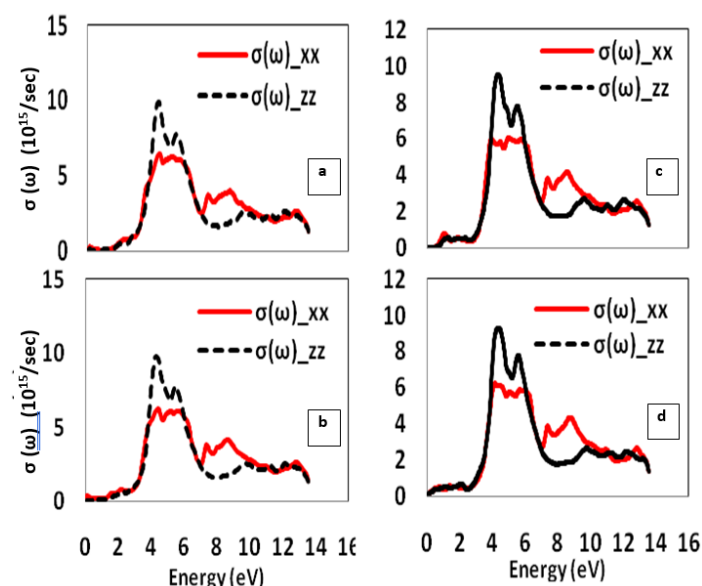


**Figure 10.** Variation of optical conductivity,  $\sigma(\omega)$  with photon energy along x- and z- directions for (a) TITbS<sub>2</sub> (b) TIDyS<sub>2</sub> (c) TIHoS<sub>2</sub> (d) TIErS<sub>2</sub>

Figures 11(a–d) give variation of energy loss of fast moving electrons through the studied materials [32]. The several peaks in energy range 0–14 eV at ~ 7.0 eV, ~8.0 eV, 11.0 eV and ~ 12.0 eV along x-direction and at ~ 9.0 eV, 11.0 eV and 12 eV along z-direction are correspond to excitation of one or more Plasmons by electrons passing through the materials. The peaks at ~ 7.0 eV, 8.0 eV, 11.0 eV and ~ 12.0 eV along x-direction and at ~ 9.0 eV, 11.0 eV and 12 eV along z-direction are due to plasma resonances associated with the collective oscillation of the electrons in the valence band [32].

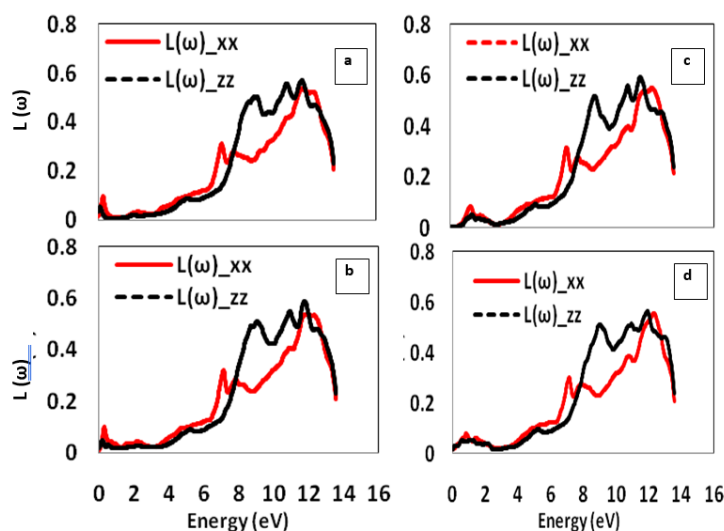


**Figure 11.** Variation of energy loss,  $L(\omega)$  with photon energy along along x- and z- directions for ((a) TITbS<sub>2</sub> (b) TIDyS<sub>2</sub> (c) TIHoS<sub>2</sub> (d) TIErS<sub>2</sub>

### 3.3 Thermodynamic Properties

Under a particular model known as the quasi-harmonic Debye (QHD) model, the impact of temperature on the thermodynamic parameters such as bulk modulus ( $B$ ), specific heat ( $C_v$ ), entropy ( $S$ ), and Debye temperature ( $D$ ) was investigated. Gibbs function, according to QHD, may be expressed as [33, 34];

$$G \times (V, P, T) = E(V) + PV + A_{vib}(\theta_D(V), T) \quad (9)$$

Where total energy per unit cell, vibration Helmholtz free energy, and Debye temperature are referred to as  $E(V)$ ,  $A_{vib}$  and  $\theta_D$ , respectively.

Under equilibrium condition, various physical thermodynamic parameters can be achieved by minimizing the Gibbs function, expressed in equation (9) with respect to volume of the unit cell at constant pressure and temperature. Here, it is for remembering that we have displayed temperature dependent thermodynamic properties only for TlTbS<sub>2</sub> and thermodynamic properties for other compounds viz. Tl(Dy/Ho/Er) have not been displayed because they show same variation with temperature as that of TlTbS<sub>2</sub>. Only the quantitative differences mentioned by Table 4 distinguish them from one another.

**Table 4.** Thermodynamic parameters viz. volume, Bulk modulus, Debye temperature, thermal expansion coefficient (at 300K) for TlRES<sub>2</sub>, RE= Tb-Er using PBE-GGA

Compounds	a	c	V (Å <sup>3</sup> )	B (GPa)	C <sub>v</sub> (J/molK)	S (J/molK)	θ <sub>D</sub> (K)	α (10 <sup>-5</sup> J/molK)
TlTbS <sub>2</sub>	4.020	2.224	731	50.30	95	100	234	5.5
TlDyS <sub>2</sub>	3.998	2.241	726.5	48.75	95	160	229	6.5
TlHoS <sub>2</sub>	4.011	2.249	721.5	50.2	95	160	230.5	6.0
TlErS <sub>2</sub>	3.961	2.244	715.0	49.25	95	160	229.5	5.5

The fluctuation of unit cell volume,  $V$ , with change in temperature is shown in Figure 12 (a). As can be observed from Figure 12 (a), the volume of a unit cell grows as temperature rises since the atomic distance likewise rises with temperature (i.e., expansion of the unit cell's dimensions happens with temperature).

The variation of bulk modulus,  $B$ , with change in temperature is seen in Figure 12 (b). Bulk modulus of a material expresses the elasticity of a material and inversely shows the compressibility of a material [35]. It can be observed from Figure 12 (b) that  $B$  decreases with temperature. The decrease in bulk modulus with temperature can be explained as: Bulk modulus is the ratio of infinitesimal stress to volumetric strain. When temperature increases, the molecules of the compounds vibrate at faster rate due to which atomic force decreases and hence bulk modulus decreases with temperature. As bulk modulus decreases with temperature, the compressibility increases i.e., TlRES<sub>2</sub> compounds become more compressible with increasing the temperature.

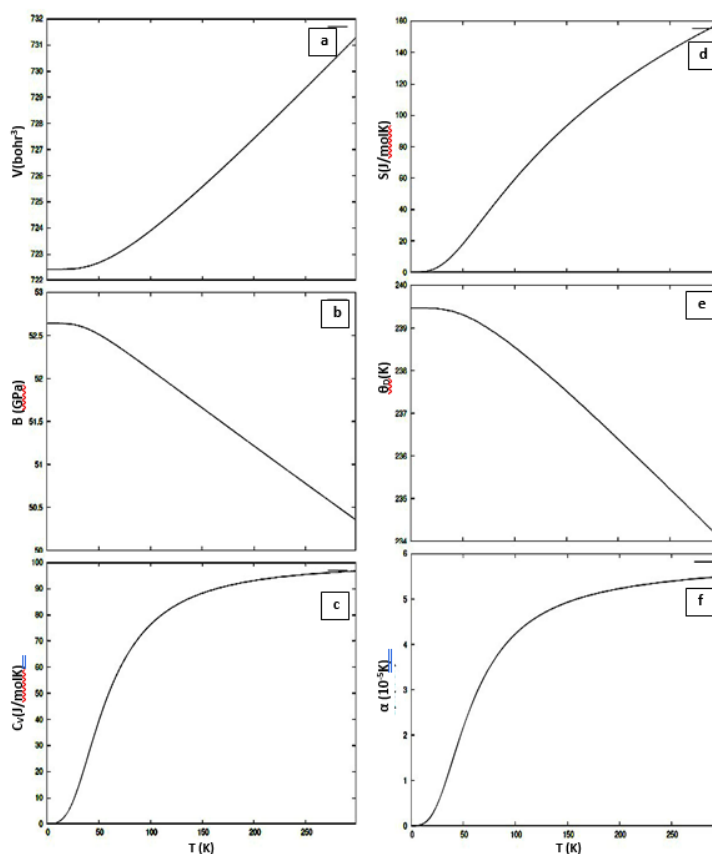
Figure 12 (c) shows the variation of specific heat at constant volume, ( $C_v$ ) with temperature. It can be seen from the Figure 12 (c) that  $C_v$  increases almost linearly upto  $T \sim 100$  K and then starts to squash. At  $T \sim 150$ K,  $C_v$  become almost constant. It indicates that atoms/molecules of studied compounds absorb more heat in the low temperature range ( $T \sim 0-150$ K) (follows Debye  $T^3$  Law) for vibration. Beyond 150K, the average kinetic energy of atoms/molecules become saturated so that  $C_v$  become saturate (approaches to Dulong-Petit law). The estimated maximum value of  $C_v$  were found to be  $\sim 95$  J mol<sup>-1</sup>K<sup>-1</sup>, indicate good absorber of thermal heat in low temperature [36].

Figure 12 (d) represents the variation of entropy ( $S$ ) with respect to temperature for TlTbS<sub>2</sub>. Entropy of a system measures the disorder of the system. Entropy directly depends upon the heat given to the system. As temperature increases by giving the heat to the system the molecules vibrate at faster rate and hence produce more disorder. Thus, entropy increases with temperature. In our case of TlTbS<sub>2</sub> (or TlRES<sub>2</sub>), the entropy (disorder) was found to be increases at faster rate.

Figure 12 (e) represents the variation of Debye temperature ( $\theta_D$ ) with temperature. The variation of Debye temperature shows decrement in  $\theta_D$  with temperature at slow rate, indicates hardness of TlRES<sub>2</sub> decreases at slow rate with temperature. It can be seen from Table 2 that TlRES<sub>2</sub> compounds have Debye temperatures in range 223–237K (not so large enough), indicate that TlRES<sub>2</sub>, are not so hard enough and they have low thermal conductivity [37]

Figure 12 (d) shows the variation of thermal expansion coefficient,  $\alpha$  with temperature. It can be observed from this figure that  $\alpha$  increase with temperature, indicate increase in fractional volume of the TlRES<sub>2</sub> compounds with temperature. It can be seen from Table 4 that  $\alpha$  ranges from  $2 \times 10^{-5}$  J/molK to  $8.5 \times 10^{-5}$  J/molK. The large

value of  $\alpha$  indicate low dimensional stability with respect to temperature i.e., TIRES<sub>2</sub> are not so hard materials [38].



**Figure 12.** Temperature dependent variation of (a) unit cell volume (b) bulk modulus (c) specific heat (d) entropy (e) Debye temperature (f) thermal expansion coefficient for TITbS<sub>2</sub>

## 4. Conclusions

A scheme FP-LAPW + lo using PBE-GGA has been applied to study the electronic, magneto-optical spectra and thermodynamic properties of TIRES<sub>2</sub> compounds. Electronic structure and magnetic characteristics show that TIRES<sub>2</sub> (RE: Tb - Er) are the half metallic ferromagnets with dominant character of spin down orbit electrons for Tl(Tb/Dy/Ho/Er)S<sub>2</sub> at the Fermi level. TIRES<sub>2</sub> compounds show 100% spin polarization of electrons at the Fermi level which is basic condition of half metallic compounds. Optical spectra show that intraband transitions occur in infrared (IR) regime due to metallic character of TIRES<sub>2</sub> and they behave as opaque in ultraviolet (UV) region. High refractive index in IR regime also show metallic character and high peak in UV regime shows slow propagation of light in UV regime. The maximum reflection coefficient ~50–60% is found in UV regime. Higher energy sides that correlate to the stimulation of one or more Plasmons by electrons travelling through the compounds been discovered to have significant energy loss. Plasma resonances lead to the frequent peaks at ~7.0 eV, 9.0 eV, 11 eV, and 12 eV. The quasi-harmonic Debye model has been used to calculate the thermodynamic characteristics of TIRES<sub>2</sub>. Thermodynamic properties show that TIRES<sub>2</sub> compounds are dimensional less stable (no so hard enough) with low thermal conductivity and disordered with temperature at faster rate.

## Acknowledgments

One of the authors, Rishi P Singh, wants to acknowledge the financial support received from Department of Science and Technology, New Delhi (under the scheme, DST-FIST scheme via project no. SR/FST/COLLEGE-318/2016).

## Conflict of interest

There is no conflict of interest for this study.

## References

- [1] Fomina K A, Marchenkov V, Shreder E I, and Weber H W. Electrical and optical properties of X<sub>2</sub>YZ (X= Co, Fe; Y= Cr, Mn, Ti; Z= Ga, Al, Si) Heusler alloys. *Solid State Phenomena*, 2011; 168: 545-548.
- [2] Fong C Y, Pask J E, and Yang L H. *Half-metallic materials and their properties*, Vol. 2, 2013; World Scientific.
- [3] Prinz G A. Spontaneous Spin Polarization of Electrons by Diluted Magnetic Heterostructures. *Physics Today*, 1995; 48: 58.
- [4] Wolf, S.A.; Awschalom, D.D.; Buhrman, R.A.; Daughton, J.M.; von Molnár, S.; Roukes, M.L.; Chtchelkanova, A.Y.; Treger, D.M. Spintronics: A Spin-Based Electronics Vision for the Future. *Science* **2001**, *294*, 1488–1495, <https://doi.org/10.1126/science.1065389>.
- [5] Şaşıoğlu, E.; Sandratskii, L.M.; Bruno, P.; Galanakis, I. Exchange interactions and temperature dependence of magnetization in half-metallic Heusler alloys. *Phys. Rev. B* **2005**, *72*, 184415, <https://doi.org/10.1103/physrevb.72.184415>.
- [6] Zhang M, Liu Z, Hu H, Liu G, Cui Y, Chen J, and Xiao G. Is Heusler compound Co<sub>2</sub>CrAl a half-metallic ferromagnet: electronic band structure, and transport properties. *Journal of magnetism and magnetic materials*, 2004; 277(1-2): 130-135.
- [7] Antonov, V.N.; Harmon, B.N.; Yaresko, A.N. Electronic Structure and Magneto-Optical Properties of Solids. **2004**, <https://doi.org/10.1007/1-4020-1906-8>.
- [8] Everhart, W.; Newkirk, J. Mechanical properties of Heusler alloys. *Helvion* **2019**, *5*, e01578, <https://doi.org/10.1016/j.helivon.2019.e01578>.
- [9] Sankar C R, Bangarigadu-Sanasy S, and Kleinke H. Thermoelectric Properties of TlGdQ<sub>2</sub> (Q= Se, Te) and Tl<sub>9</sub>GdTe<sub>6</sub>. *Journal of Electronic Materials*, 2012; 41(6): 1662-1666.
- [10] Duczmal, M.; Mosiniwicz-Szablewska, E.; Pokrzywnicki, S. Electron paramagnetic resonance of Gd<sup>3+</sup> in TlGdSe<sub>2</sub>. *Phys. Status solidi (a)* **2003**, *196*, 321–324, <https://doi.org/10.1002/pssa.200306417>.
- [11] Gautam R, Kumar A, and Singh R. First Principle Investigations on Electronic, Magnetic, Thermodynamic, and Transport Properties of TlGdX<sub>2</sub> (X= S, Se, Te). *Acta Physica Polonica A*, 2017; 132(4): 1371-1378.
- [12] Duczmal, M.; Pawlak, L. Magnetic and structural characterization of TlLnSe<sub>2</sub> compounds (Ln = Nd to Yb). *J. Alloy. Compd.* **1995**, *225*, 181–184, [https://doi.org/10.1016/0925-8388\(94\)07082-2](https://doi.org/10.1016/0925-8388(94)07082-2).
- [13] Duczmal M, and Pawlak L. Magnetic properties of TlLnS<sub>2</sub> compounds (Ln≡ Tb, Ho and Tm). *Journal of Alloys and Compounds*, 1995; 219(1-2): 189-192.
- [14] Guseinov G D, Abdullayev G B, Bidzinova S M, Seidov F M, Ismailov M Z, and Pashayev A M. On new analogs of TlSe-type semiconductor compounds. *Physics Letters A*, 1970; 33(7): 421-422.
- [15] Blaha P, Schwarz K, Sorantin P, and Riskey S B. *Comput. Phys. Commun*, 1990; 59: 399.
- [16] Blaha, P.; Schwarz, K.; Madsen, G.K.H.; Kvasnicka, D.; Luitz, J. WIEN2k, An Augmented Plane Wave + Local Orbitals Program for Calculating Crystal Properties. Karlheinz Schwarz, Technische Universität Wien, Austria, 2001, ISBN 3-9501031-1-2.
- [17] Mun Wong K, Alay-e-Abbas S M, Shaikat A, Fang Y, and Lei Y. First-principles investigation of the size-dependent structural stability and electronic properties of O-vacancies at the ZnO polar and non-polar surfaces. *Journal of Applied Physics*, 2013; 113(1): 014304.
- [18] Wang, V.; Xu, N.; Liu, J.-C.; Tang, G.; Geng, W.-T. VASPKIT: A user-friendly interface facilitating high-throughput computing and analysis using VASP code. *Comput. Phys. Commun.* **2021**, *267*, 108033, <https://doi.org/10.1016/j.cpc.2021.108033>.
- [19] Perdew, J.P.; Burke, K.; Ernzerhof, M. Generalized gradient approximation made simple. *Phys. Rev. Lett.* **1996**, *77*, 3865–3868. <https://doi.org/10.1103/PhysRevLett.77.3865>.
- [20] Kohn W, and Sham L J. *Phys. Rev. B*, 1996; 140A: 1133.
- [21] Ehrenreich, H.; Cohen, M.H. Self-Consistent Field Approach to the Many-Electron Problem. *Phys. Rev.* **1959**, *115*, 786–790, <https://doi.org/10.1103/physrev.115.786>.
- [22] Hedin L. New method for calculating the one-particle Green's function with application to the electron-gas problem. *Physical Review*, 1965; 139(3A): A796.
- [23] Fox M. 2002; *Optical properties of solids*.
- [24] Abeles F. 1972; *Optical Properties of Solids*. USA: American Elsevier.
- [25] Wang H, Wang Y, Cao X, Zhang L, Feng M, and Lan G. Simulation of electronic density of states and optical properties of PbB<sub>4</sub>O<sub>7</sub> by first-principles DFT method. *physica status solidi (b)*, 2009; 246(2): 437-443.

- [26] Duczmal M. Structure, magnetic properties and crystal field in triple lanthanide chalcogenide and thallium  $TlLnX_2$  ( $X = S, Se$  or  $Te$ ). 2003; Wrocław, Poland: Publishing House of the Wrocław University of Technology.
- [27] Chand S, Singh R P, Govindan A, and Singh S K. Mechanical, spin polarized electronic and magnetic properties of  $TmX$  ( $X = Cu, Ag$ ): first principle study. *International Journal of Modern Physics B*, 2015; 29(03): 1550007.
- [28] Joshi, H.; Rai, D.P.; Hnamte, L.; Laref, A.; Thapa, R. A theoretical analysis of elastic and optical properties of half Heusler  $MCoSb$  ( $M = Ti, Zr$  and  $Hf$ ). *Helvion* **2019**, 5, e01155, <https://doi.org/10.1016/j.helivon.2019.e01155>.
- [29] Penn D R. Wave-number-dependent dielectric function of semiconductors. *Physical review*, 1962; 128(5): 2093.
- [30] Bhamu K C, Khenata R, Khan S A, Singh M, and Priolkar K R. Electronic, optical and thermoelectric properties of  $2H-CuAlO_2$ : A first principles study. *Journal of Electronic Materials*, 2016; 45: 615-623.
- [31] Dresselhaus M S. Solid state physics part ii optical properties of solids. Lecture Notes (Massachusetts Institute of Technology, Cambridge, MA), 2001; 17: 15-16.
- [32] Wooten F. Optical properties of solids. *American Journal of Physics*, 1973; 41(7): 939-940.
- [33] Blanco, M.; Francisco, E.; Luaña, V. GIBBS: isothermal-isobaric thermodynamics of solids from energy curves using a quasi-harmonic Debye model. *Comput. Phys. Commun.* **2004**, 158, 57–72, <https://doi.org/10.1016/j.comphy.2003.12.001>.
- [34] Otero-de-la-Roza A, Abbasi-Pérez D, and Luaña V. Gibbs2: A new version of the quasiharmonic model code. II. Models for solid-state thermodynamics, features and implementation. *Computer Physics Communications*, 2011; 182(10): 2232-2248.
- [35] Kumar N, Kumar S, Yadav K, Kumar A, Singh P K, Srivastava N, and Singh R P. Study on thermodynamic, electronic and magnetic properties of  $RE_2Cu_2Cd$  ( $RE = Dy-Tm$ )  $RE_2Cu_2Cd$  ( $RE = Dy-Tm$ ) intermetallics: first-principle calculation. *Bulletin of Materials Science*, 2020; 43: 1-9.
- [36] Kumar A, Guatam R, Chand S, Kumar A, and Singh R P. First principle electronic, magnetic and thermodynamic characterization of heavy fermion ternary rare earth metal alloys. *Materials Physics & Mechanics*, 2019; 42(1): 112-130.
- [37] Li, C.; Wang, Z. Computational modelling and ab initio calculations in MAX phases – I. **2012**, 197–222, <https://doi.org/10.1533/9780857096012.197>.
- [38] Biron M. Detailed Accounts of Thermoplastic Resins. In *Thermoplastics and Thermoplastic Composites* (Third Edition), 2013.